The FANCM family Mph1 helicase localizes to the mitochondria and contributes to mtDNA stability

Manuel Bernal, Xuejiao Yang, Michael Lisby, Gerard Mazón

An article to DNA Repair

The FANCM family Mph1 helicase localizes to the mitochondria and contributes to mtDNA stability

Manuel Bernal [1], Xuejiao Yang[2,3], Michael Lisby[2] and Gerard Mazón [1*]

[1] CNRS UMR8200 – Genetic Stability and Oncogenesis, Université Paris-Sud, Paris-Saclay, Institut Gustave Roussy, Villejuif (France)

[2] Department of Biology, University of Copenhagen, DK-2200 Copenhagen N, Denmark.

[3] Current address: Department of Cancer Biology, Basser Center for BRCA, Perelman School of Medicine, University of Pennsylvania, Philadelphia, Pennsylvania 19104, USA

[*]Corresponding author: gerard.mazon@gustaveroussy.fr

Keywords: Mitochondrial DNA repair, Helicase Mph1, Fanconi Anemia-like pathway, Double-strand break, Homologous Recombination

Abstract

Mitochondria are membrane-bound organelles found in eukaryotic cells where they generate energy through the respiratory chain. They contain their own genome that encodes genes critical to the mitochondrial function, but most of their protein content is synthetized from nuclear encoded genes. Damages to the mtDNA can cause mutations and rearrangements with an impact on the respiratory functions of the cell. DNA repair factors are able to localize to mitochondria to restore mtDNA integrity and ensure its proper inheritance. We describe in this article the mitochondrial localization of the Mph1/FANCM helicase that serves critical roles in nuclear DNA repair processes. Mph1 localizes to mitochondria and its functions contribute to the mtDNA integrity under mtDNA damaging conditions.

1. Introduction

Members of the FANCM family of DNA translocases/helicases play important roles in the maintenance of the genome integrity. Both the human FANCM and its yeast orthologue Mph1 preferentially bind substrates containing branched DNA such as Replication Forks (RFs) and D-loops [1]. In budding yeast, Mph1 plays important roles in fork remodeling and allows repair of lesions during replication [2-4]. During double-strand break (DSB) repair by homologous recombination, Mph1 has been shown to use its helicase activity to directly unwind D-loop intermediates promoting its early displacement and thereby avoiding crossover formation [1]. Mph1 anti-crossover function during DSB repair is directed to substrates similar to those of the Mus81-Mms4 nuclease, and the presence of both players is critical to survive nuclear DNA DSBs and to avoid accumulation of branched intermediates [3].

Mitochondria are eukaryotic organelles that contain multiple copies of mitochondrial DNA (mtDNA). mtDNA is organized in nucleoids that are in close proximity to the respiratory chain at the inner membrane and thus are highly susceptible to oxidative damage [5, 6]. mtDNA codes for several subunits of the respiratory chain, and unrepaired damage may rapidly lead to respiratory chain dysfunctions that would aggravate the oxidative stress situation [7, 8]. To counter the negative effects of mtDNA damage, mitochondria have kept several operational DNA repair pathways through evolution, including double-strand break repair [7, 9, 10]. In yeast, dual targeting [11] allows proteins like Ntg1, Pif1 and several *RAD52* epistasis group proteins to be used both in the nucleus and in the mitochondria [12-14] while some other mitochondrial DNA repair proteins such as Cce1, Mhr1 or Din7 are encoded in the nucleus but are only localized in the mitochondria [15-17]. Although these evidences strongly support the presence of DNA repair mechanisms in the mitochondria it might also be possible that in some situations, together with repair mechanisms, cells counter deleterious effects of mitochondrial DNA damage by degradation of the damaged mtDNA and amplification of the undamaged mtDNA [5]. In yeast, two modes of mtDNA replication mechanisms have been proposed

[18, 19]. Transcription-dependent replication uses RNA transcripts as primers for DNA replication in a mechanism that is not essential for mtDNA inheritance [20-24]. In parallel, transcription-independent mechanisms can amplify mtDNA by a rolling-circle mechanism from its *ori5* in a DSB-dependent manner [25], with a critical role of the Ntg1 base-excision repair enzyme [26] that cleaves the DNA at the *ori5* region, which is preferentially damaged by reactive oxygen species (ROS) or other DNA damage insults to initiate the recombination bubble at the origin of the rolling-circle [16, 27-29].

Mph1 has been described as an exclusively nuclear protein [2, 30, 31], but its association to proteins that are strictly mitochondrial or in its vast majority mitochondrial [32-35] raises the question of whether Mph1 has the ability as well to localize to mitochondria and exert functions in preserving mtDNA stability. SILAC co-immunoprecipitation (co-IP) suggested that Mph1 is able to interact with the Ssb-like protein Rim1 and the Rad52-like protein Mgm101 [32]. Rim1, an essential protein for mitochondrial DNA replication, is mostly accepted to be an exclusively mitochondrial protein [36] and its Mph1 interaction might only be possible if Mph1 localizes to mitochondria. Mgm101 is a Rad52-family protein that allows ssDNA annealing and plays a role in the mitochondrial repair of oxidative DNA damage and in mitochondrial recombination [33, 37]. Besides its mitochondrial functions, Mgm101 was proposed to play a role during ICL repair as part of a FA-like pathway in the nucleus [31], where a fraction of Mgm101 might be able to localize [34].

In this article, we describe how the Mph1 helicase is able to localize to the mitochondria, where it is involved in the mechanisms of mtDNA maintenance. Mph1 adds to the set of nuclear DNA repair proteins able to localize to mitochondria and suggests that the FA pathway and its FA-like pathway in yeast take part in the mitochondrial genome homeostasis, raising interesting possibilities of how a perturbed FA pathway may have an impact in the cell catabolism and its oxidative burden.

2. Materials and Methods

2.1. Yeast Strains and Growth Conditions

Saccharomyces cerevisiae strains and plasmids used in this study are listed in Supplementary Table 1. The plasmid expressing the mitochondrial-targeted *Xho*I endonuclease was provided by Dr. Lynn Harrison and used material provided by New England Biolabs [38]. The *MPH1*-1xFLAG-1xHA (Mph1-F-HA) allele was generated by inserting at the Mph1 C-terminus a single -FLAG epitope and a single -HA epitope separated by a FactorXa site with dedicated oligonucleotides listed in Supplementary Table 2. Mutants in the different designated loci were obtained by gene replacement with the indicated selective cassettes and crossing. Cells were typically grown in YP (1% yeast extract; 2% peptone) or SC media with 2% glucose (YP-D) or 3% glycerol (YP-G). Strains with induced protein expression were grown in YP-G supplemented with 2% galactose. Methyl methane sulfonate (MMS, Sigma), Zeocin (Zeo, Invitrogene) and 4-Nitroquinoline 1-oxide (4-NQO, Sigma) were added to the different media at the designated doses for DNA damage sensitivity assays.

2.2. Western Blot analyses

Trichloroacetic acid (TCA) precipitations were performed on whole cell extracts and were analyzed by SDS-PAGE and Western blotting. Samples were loaded onto 7.5% or 4-15% gradient Tris-Glycine BioRad stain-free pre-casted gels for routine analysis and hybridized on TBST 5% milk with the appropriate antibodies. Antibodies were used at the suggested dilutions: anti-HA-HRP (3F10, Roche) 1:1,000, anti-Pgk1-HRP (ab113687, Abcam) 1:5,000, anti-Tim23 (sc-14046, Santa Cruz) 1:1,000, anti-Histone H2B (ab188291, Abcam) 1:2,000, anti-FLAG-HRP (A8592, Sigma), 1:2,000, anti-Rad53 (ab104232, Abcam) 1:2,000. When required, secondary anti-Rabbit-HRP and anti-Goat-HRP antibodies (Cell Signaling) were used at 1:5,000 and 1:10,000 respectively. Western blots were revealed with WesternBright ECL solution (Advansta) or WesternBright Sirius HRP substrate if required (Advasta).

2.3. Sucrose gradient fractionation

For sucrose density gradient fractionation and purification of mitochondrial fractions 500 ml cultures of the different strains were grown to OD_{600} 0.8 in YP-D or SC-URA 3% Glycerol. When indicated, mt*Xho*I was induced with addition of Galactose to 2% for 2.5h. The fractionation of yeast cell extracts followed the previously published protocol [39] with few modifications. Cells were harvested and resuspended in 7 ml Lysis Buffer (20 mM potassium phosphate (pH 7.4), 1.2 M sorbitol, 1 mg Zymolyase (Zymo Research)) per gram of wet pellet. After incubation at 30ºC for 30 minutes, spheroplasts were collected by 5 minutes centrifugation at 2200 g at 4ºC. Spheroplasts were then resuspended in 7ml of cold Homogenization Buffer per gr of wet pellet (10 mM Tris/HCl (pH 7.4), 0.6 M sorbitol, 1 mM EDTA, 0.2% (w/v) BSA) and lysed at 4ºC in a glass homogenizer (15 strokes of the pestle for every 6 ml of homogenized spheroplasts). Nuclei and cytoplasmic fractions were separated by centrifugation at 1500 g. Crude mitochondria were pelleted from the soluble fraction at 12000 g and suspended in 6 ml of cold SEM Buffer (10 mM MOPS/KOH (pH 7.2), 250 mM sucrose, 1 mM EDTA). Crude mitochondrial fractions were further purified in a sucrose gradient (4 layers w/v 60-32-23-15%) in EM buffer (10 mM MOPS/KOH (pH 7.2), 1 mM EDTA) by 1h centrifugation at 134000 g with a SW41Ti rotor. The pure mitochondrial fraction was recovered and pelleted at 34400 g for 60 minutes at 4ºC in a TLA 100.3 rotor, resuspended in 80 µl of SEM buffer and subjected to analysis by WB following standard TCA protocol.

2.4. Survival curves and DNA sensitivity assays

Cells were grown in YP-G to select for functional mitochondria before measuring DNA damage sensitity and clonogenic survival. To measure DNA damage sensitivity, 10-fold serial dilutions of equal amounts of cells were spotted onto plates containing the indicated doses of genotoxic agents in Glucose or Glycerol containing media. Growth was monitored at 2 and 3 days. For clonogenic survival curves, strains were diluted and an equal number of cells were plated for the different conditions to estimate survival by

comparing colony-forming units after 3 days in untreated and treated conditions.

2.5. Induction of mtDSB and analysis of respiration competence

Cells harboring either a plasmid expressing mt*Xho*I or mtRFP [38] were grown in SC-URA media (Glycerol 3%) and mtDSB induction or its mock control was achieved by addition of Galactose (2%). Cells were plated in YP-D media to allow recovery from mtDSBs under non-selective conditions for respiratory growth and after 2 days colonies were replica-plated to YP-G (Glycerol 3%) to monitor the respiration deficient colonies (absence of growth). The same scheme of induction was used to monitor cell extracts by sucrose gradient fractionation to compare the mitochondrial Mph1 fraction in the presence or absence of specific mtDSBs.

2.6. BiFC-based protein-protein interaction (PPI) screen

Bimolecular fluorescence complementation (BiFC) analysis was based on the YFP variant Venus [40, 41]. In brief, genes were fused at their 3´-end to sequences encoding either the C-terminal fragment of Venus (VC) or the N-terminal fragment of Venus (VN) to examine interaction between two proteins leading to emission of yellow fluorescence [42]. In the BiFC-based PPI screen for Mph1, a query strain (XY1) containing VC-tagged Mph1, was mated with a library of 5809 strains individually expressing a VN-tagged open reading frame (ORF). The resulting diploids were selected on SC-Met-Trp and then sporulated as described [43]. Next, haploid cells expressing Mph1-VC, NLS-RFP and VN-tagged query protein were selected on SC-Leu-Ura-Lys-His-Arg containing 50 mg/L canavanine, 50 mg/L thialysine and 100 mg/L nourseothricin. The haploid cells were inoculated into 150 µl SC+Ade medium in 96-well plates, grown overnight at 30°C, and diluted 20-fold into 384-well CellCarrier plates (PerkinElmer) for examination by automated high-throughput fluorescence microscopy (PerkinElmer Opera QEHS). One second exposure time for each channel was used. Data analysis was performed using Columbus software (PerkinElmer).

2.7. Microscopy and Cell Biology Methods

Live cell imaging of Mph1-YFP and selected BiFC interactions were performed with a Spinning Disk Confocal Microscope (CSU-W1, Yokogawa), with an electron multiplying charge device camera (ANDOR Zyla sCMOS) and a 60x/1.35 numerical aperture objective at 30ºC. Cells were mounted on agarose pads as described [44] and imaging recorded 15 z-sections with 0.5 µm spacing. Image acquisition was performed using Fiji (ImageJ) [45]. Cells were grown in synthetic complete or SC-Ura medium for routine observation of cells harboring *MPH1*-YFP or detailed BiFC analysis.

2.8. Quantitative PCR analysis and RT-PCR analysis

For qPCR analysis, total DNA extracted from overnight cell cultures in SC-URA with 3% Glycerol were used as a reference for total mitochondrial and nuclear DNA. Cells grown in SC-URA 3% Glycerol were induced for mt*Xho*I and released in 5 ml of YPD media for an overnight growth. In all the reactions 10 ng of total DNA were mixed with qPCR master mix (Promega GoTaq) and the indicated primers (see Supplementary Table 2) to amplify a ≈150 bp fragment of *COX1* or *ACT1*. The relative amount of both markers was used to calculate the copies of mitochondrial DNA relative to nuclear DNA.

For RT-PCR, RNA TRIzol (Thermo Fischer) extractions were performed following the manufacturer's protocol. RNA was subjected to reverse-transcriptase amplification using Titan One Tube RT-PCR (Roche) with oligonucleotides at the -77 (FW) and +395 (RV) position from the Mph1 start codon (+1) or a pair of oligonucleotides amplifying a fragment of similar size in *BIM1* as control (see Supplementary Table 2). The putative second start site in Mph1 (Met^{111}) would have the start codon at +331/333, any spliced form of the mRNA to allow expression of such isoform will allow amplification of fragments <472bp. A standard PCR reaction was performed as quality control of RNA extractions to rule out the presence of DNA.

2.9. Southern blot analysis of mtDNA

To analyze the generation of DSBs in the mtDNA by *Xho*I, a culture of a wild-type strain harboring the plasmid expressing mtXhoI was grown in SC-URA (3% Glycerol) and Galactose was added to induce the expression of mtXhoI for 2.5h. The induction was halted by the addition of Glucose at 2% and the culture was still monitored for 3 hr. At different time intervals, samples of 100ml were collected and total DNA was extracted using phenol-chloroform extraction and ethanol precipitation. Total DNA from the different samples were digested over-night with *Hind*III and *Pvu*II and migrated in 0.5% agarose gels at 150V for 3hrs in TBE 0.5X buffer. The gels were transferred to nylon membranes (GE Amersham Hybond-N) by capillarity in 10X SSC and hybridized at 60ºC with the appropriate probes (*COX1, VAR1/21S* and *BIM1*) labeled with ^{32}P with a random priming kit (Roche). Images were obtained after the exposition of the membranes to a phosphor-screen (GE Healthcare) and the detection by a Typhoon FLA 5200 scanner (GE Healthcare). Band intensities were quantified using Image Lab 6.0.1 (BioRad).

3. Results and Discussion

3.1. A fraction of the Mph1 protein pool localizes to the mitochondria

In addition to the previously described interactions of Mph1 to mitochondrial proteins [31, 32, 35], we screened for additional putative Mph1 mitochondrial interactions using a BiFC library, which revealed the mitochondrial proteins Ecm18 and Pda1 (summarized in Table 1). Through BiFC, two proteins that putatively interact are tagged with two domains of the Venus fluorescent tag. Only in close proximity, the two Venus domains will interact to re-constitute the fully folded and fluorescent protein [41]. BiFC thus allows detection of fluorescence in the location and the near-immediate moment of the protein's interaction. To determine the precise subcellular localization of some of these interactions by BiFC, a strain expressing the *MPH1–VC* allele from the endogenous locus was crossed to strains containing either *MGM101-VN* or *RIM1-VN*. The resulting diploids were analysed for BiFC signal in SC media with or without induction of highly specific

mitochondrial DNA double-strand breaks generated by expressing a mitochondrial-targeted *Xho*I nuclease under control of a galactose-inducible promoter [38]. *Xho*I has two cleavage sites in the mitochondrial genome (Figure 1A). In 5.6% (±3.6%) of negative control cells without the BiFC tags, we detected a signal at 488 nm co-localizing with the MitoTracker signal. By comparison, the fraction of cells with a BiFC signal increased to 14% (±1.6%) in cells expressing *MPH1-VC* and *MGM101-VN*, and further increased to 25.2% (±2%) after induction of mtDSBs, significantly above the 10% (±0.7%) of BiFC-positive control cells observed when induced for mtDSBs (Figure 1A and 1B). Cells expressing *MPH1-VC* and *RIM1-VN* did not present a mitochondrial BiFC above background in unchallenged conditions, but we detected a BiFC signal in 18.8% (±2.3%) of the cells after mtDSB induction (Figure 1A and 1B).

An endogenous *MPH1–YFP* allele allows the direct monitoring of Mph1 sub-cellular localization, but barely above the detection limits. In these conditions, observation of Mph1-YFP in cells growing in normal conditions (no mitochondrial damage) didn't allow us to detect significant signal inside the mitochondria (Figure 1C), suggesting that the amount of mitochondrial Mph1 is lower than its nuclear pool and possibly transient. Notably, 14.2% (±0.6%) of the cells showed Mph1-YFP foci co-localizing with the mitochondrial network after 2.5h induction of mt*Xho*I with galactose compared to the background of auto-fluorescence foci in 4.7% of cells in the same condition of mt*Xho*I induction (Figure 1C, S1), indicating that Mph1 is recruited to sites of mitochondrial DNA damage.

To further confirm that Mph1 is able to localize to mitochondria as suggested by the microscopy observations of Mph1-YFP, we purified mitochondria from a strain that expresses Mph1-F-HA from the endogenous locus by sucrose gradient fractionation and we analysed the mitochondrial fraction by western blotting. The Mph1 protein was clearly detected in the mitochondrial fraction, although the mitochondrial fraction was minor as compared to the whole cell extract suggesting the majority of Mph1 localizes to the nucleus (Figure 2A). We next investigated if the pool of mitochondrial Mph1 was increased

after induction of specific mitochondrial DNA damage by comparing the levels of Mph1 with or without induction of the mt*XhoI* nuclease (Figure 2B). Mitochondrial Mph1 levels normalized to Tim23 mitochondrial loading control remained stable after 2.5h of mt*Xho*I expression, suggesting no massive import of Mph1 occurs after induction of mtDNA damage.

3.2. A putative internal Mitochondrial Targeting Signal (MTS) has the ability to direct Mph1 to the mitochondria

Mitochondrial proteins are able to localize to the organelle by specific transport signals known as Mitochondrial Targeting Signals (MTS). These signals are normally N-terminal and consist of positively charged amphipathic α helices with a significant number of basic residues and a net positive charge [46-48]. Most of the canonical mitochondrial proteins possess these types of N-terminal signals, and likewise proteins with a nuclear localization may specifically be imported to the mitochondria by exposing internal MTS under certain conditions of stress or after modifications in its translated sequence (reviewed in [49-52]). Indeed, by querying Mph1 sequentially from its N-terminus for the presence of putative MTS, we found that the region between Arg-88 and Arg-180 possesses helices able to constitute an MTS-like domain (Figure 3A). Translation from a putative second start codon present at Met-111 was predicted to generate a protein with a high score for mitochondrial localization (Figure 3A) and forced translation from Met-111 generated an Mph1 variant that localized in its vast majority to the mitochondria (Figure 3B). To examine the possibility that alternatively processed mRNAs were produced to generate a Mph1 isoform starting at Met-111, we performed a RT-PCR analysis of *MPH1's* mRNA (Figure 3C). We were not able to detect PCR products from spliced mRNA forms of Mph1 in either normal growth conditions or growth under oxidative stress (+H_2O_2). Since the RT-PCR only detected fragments compatible with full-length mRNA, we speculated that the MTS-like domain might be used in the context of the full-size protein by specific bending or folding. In this line, we did not detect any signal by western blot of a naturally occurring Mph1

isoform with the equivalent size of a form translated from Met-111 (Figure 3D). The Mph1 protein is largely nuclear, with a putative NLS sequence in its C-terminus (821-851), if the MTS signal was constitutively exposed we would expect the protein to localize exclusively to mitochondria as does the Met-111 truncated form despite containing the functional NLS (Figure 3D). Its predominant nuclear localization suggests the internal MTS is tightly controlled to prevent a general mitochondrial translocation.

3.3. Deletion of MPH1 impacts the repair of mtDSBs

Deletion of *MPH1* has been associated so far to nuclear phenotypes during DSB repair or under replication stress, *mph1*Δ strains do not present any spontaneous mitochondrial defect or petite phenotype in unchallenged conditions [31]. We thus wondered if the putative functions of Mph1 in the mitochondria are somehow non-essential for the mtDNA stability and have to be revealed in conditions of mtDNA damage and in combination with mutations in alternative mtDNA maintenance pathways. Since Mph1 has a role dissociating joint-molecule intermediates during homologous recombination after a nuclear DSB [1, 3, 53] we first turned our attention to its putative role in the repair of induced mtDSBs.

Cells from overnight SC-URA 3% Glycerol cultures were induced for mtDSB formation with addition of Galactose to 2% or an equivalent mock induction in cells carrying a plasmid coding for an inducible mtRFP. After 2.5h induction of the mtDSB, cells were plated in YP dextrose (YP-D) media to allow growth of cells regardless of their mitochondrial status. Colonies were replica-plated in YP-G after 2 days to monitor their mitochondrial function. Cells able to grow on YP-G were scored as respiration competent and reported to the total colonies able to grow in YP-D (Figure 4A, Tables S3 and S4). Total DNA from wild-type cells expressing the mt*Xho*I was extracted at different time points to verify that the enzyme cut the mtDNA at the *Xho*I sites located in the *COX1* coding sequence and the inter-genic region between *VAR1* and the *21S* coding sequences (Figure 4B, Figure S2). A peak of mtDSB products was observed after 1h

mtXhoI induction and remained similar after 2.5h induction. Under a recovery phase where mt*Xho*I expression ceases and its protein levels decreases (Figure S3A), the amount of mtDNA (normalized to a nuclear DNA marker) was reduced representing only 8% of the initial mtDNA amount after 3h recovery growth in YP-D (Figure 4B). No significant cutting was observed in the nuclear DNA by analyzing an *Xho*I site present in the coding region of *BIM1* (Figure 4B). Moreover, the amount of mtDNA in cells subjected to 2.5h mt*Xho*I induction was drastically reduced by 8-fold as estimated by qPCR. An analysis by colony-PCR of survivors using oligonucleotides flanking the *Xho*I site in *COX1* of 25 individual colonies unable to grow in glycerol showed a vast majority (92%) of the colonies lost mtDNA integrity in this region while 2 out of 25 retained mtDNA, with its intact *Xho*I site (tested by *in vitro* digestion), but lost the respiration competence (Figure 4C). We did not detect activation of the nuclear DNA damage checkpoint during the induction of mtXhoI suggesting the XhoI nuclease was exclusively targeted to the mitochondria and had a negligible impact to the nuclear DNA stability (Figure S3B).

Yeast cells contain multiple mitochondria that in turn may contain up to 10 copies of mtDNA [18, 54]. After prolonged induction of mt*Xho*I most of the mtDNA molecules are cut and may become irreparable by recombination in the absence of intact DNA templates. Nonetheless, at the 2.5h endpoint, *mph1*Δ cells showed a moderate decrease in respiration-competent colonies after mtDSB induction compared to the wild-type strain. We next determined the genetic interactions of *mph1*Δ with deletions of *NTG1, ABF2, CCE1 and DIN7.* Interactions with *RIM1* and *MGM101* could not be tested because these deletions generate petites at a very high frequency and could not be selected in YP-G after tetrad dissection to start the experiment from a homogenous mitochondria-containing starting culture. We also analyzed the impact of a nuclear-only version of Pif1 (*pif1-m1*) that behaves as a mitochondrial deficient copy while preserving its intact nuclear functions [55].

The Cce1 resolvase cuts joint-molecule intermediates in the mitochondria [16, 56, 57], and we observed a mtDSB-induced decrease of respiration-competent colonies in

the *cce1*Δ strain, further accentuated by its combination with *mph1*Δ (Figures 4 and 5). Din7 exonuclease participates in the end-resection of the early intermediates of mitochondrial DSBs [17, 28, 58] and as expected, *din7*Δ also displayed a decrease in respiration competent colonies after induction of mtDSBs, with no further effect in a *din7*Δ *mph1*Δ strain (Figure 4A). Deletion of the *NTG1* glycosylase gene [26] also generated an mtDSB-induced decrease in respiration-competent cells, probably due to its role in triggering mtDNA amplification, not further aggravated by *mph1*Δ (Figure 4A).

Mock controls for wild-type and the different mutants were not significantly altered after mtDSB induction, except for *cce1*Δ, *abf2*Δ and *pif1-m1,* which have been already described to have a significant frequency of spontaneous petite formation. Abf2 is a DNA binding protein of the HMG1 family with an important role in the maintenance of the mtDNA nucleoid stability [59]. The rapid spontaneous loss of respiration efficiency detected in *abf2*Δ (mock conditions, Figure 4A) was in agreement with previous reports suggesting the loss of mitochondria in these mutants occurs in around 10-18 generations under non-selective conditions [7, 60]. At the 2.5h induction endpoints, *mph1*Δ further accelerated the spontaneous defects of an *abf2*Δ mutant in the mock treated cells, and after induction of mtDSBs both strains showed a homogenous petite phenotype suggesting all mtDNA loss occurred in just few generations (Figure 4A). *pif1-m1* cells carrying the mock control plasmid generated petites at a high frequency (42% of respiration competence in mock conditions), comparable to that of a *pif1*Δ allele [7]. The already high spontaneous petite formation rate was not further accelerated with the introduction of *mph1*Δ (Figure 4A), suggesting an epistatic role in preventing the spontaneous loss of the mtDNA integrity and respiration competence. Pif1 plays important roles in both mitochondrial replication and recombination [61, 62] and *pif1*-deficient cells have a reduced ability to maintain mtDNA integrity after oxidative damage [7]. After induction of mt*Xho*I, *pif1*-m1 *mph1*Δ cells displayed a further decrease in respiration competence (8.2%±2.1) compared to the *mph1*Δ strain (18.9%±4.3), but the fraction of

colonies retaining respiration competence in the *pif1-m1* single mutant were similar (8.1%±3.2) thus suggesting a dominant role for Pif1 in an epistatic relation.

We decided to further study the genetic interaction of *mph1*Δ and *cce1*Δ that appeared to be synergisitic. To confirm this point, we induced mt*Xho*I and plated cells at different time points in order to limit the number of cuts and allow its repair by recombination in conditions representing a "sub-lethal" dose of mtDSBs. In these conditions, the formation of respiration deficient colonies in the *mph1*Δ strain remained significantly higher compared to the wild-type strain with 30 min or 60 min of mtDSB induction (Figure 5). Considering that cells present about 30% of spontaneous petite formation in a *cce1*Δ background, we decided to normalize the results of mtDSB induction to the spontaneous rate of petite formation detected in mock conditions for each point of the mtDSB induction. Normalization allows a more pertinent comparison of the effects we can assign to the mtDSB response. Comparing the normalized frequencies of respiration competence after an induced mtDSB we observed that a single *cce1*Δ strain presented a similar effect to that of an *mph1*Δ, while combining *mph1*Δ and *cce1*Δ further increased the formation of petite colonies after mtDSB induction at all induction time points (Figure 5A). No further decrease in the respiration-proficient survivors was obtained by extending induction from 1h to 2.5h in any of the strains, probably reflecting that all available *Xho*I sites were cut at 1h and a slow phase of repair occurred during the recovery-phase growth in the YP-D plates, after *Xho*I turnover. Such turnover can be observed by following *Xho*I amounts during induction and recovery in cells cultured in liquid media after a 2.5h induction with galactose (Figure S3). A southern blot analysis of the kinetics of mtDSB generation in the wild-type, the single mutants and the *mph1*Δ *cce1*Δ strain showed no major differences in the degree and timing of mtDSB generation (≈40% of the molecules were cut at 1h and 2h30), further confirming that the phenotypic differences are mostly established by the different abilities to keep mtDNA during the recovery phase (Figure 5B, Figure S4). The endpoint measurement of the relative amount of mtDNA for these strains basically recapitulates the trend of the differences observed by plating.

3.4. Genetic interactions of *mph1*Δ with mtDNA maintenance genes under genotoxic stress

mtDSBs generated by *Xho*I in the mtDNA will rapidly lack donor sequences to template repair when the nuclease is highly expressed. To figure out the impact of Mph1 on mtDNA repair and mitochondrial stability in more physiological conditions, we examined the possible effects of different sources of DNA damage by comparing YP-G and YP-D growth of the different strains in the presence of genotoxic agents. Cells were grown under YP-G conditions to select for respiratory function and appropriate dilutions were plated in either YP-G or YP-D plates containing different amounts of genotoxic agents. Effects to both the nuclear and the mitochondrial DNA repair were expected to prevent cell growth in YP-D, while specific mitochondrial DNA impacts were expected to prevent cell growth only in the YP-G media by impairing the respiratory functions and leaving the viability under fermentable sources intact. Interestingly, we found some mutants to be specifically sensitive to 4-NQO at low doses (0.035-0.085 µg/ml range) on YP-G but not on YP-D, which is indicative of a mitochondrial DNA repair defect (Figure 6A). Under these conditions *mph1*Δ cells showed a small increase in sensitivity in YP-G media, and remained viable in YP-D (Figure 6A). Cells carrying *abf2*Δ had a strong sensitivity to 4-NQO under YP-G growth selection as expected by its already high spontaneous rate of mtDNA loss [59], but *mph1*Δ significantly increased its sensitivity to 4-NQO suggesting that the role of Mph1 in the mitochondria is more important in an *abf2*Δ background (Figure 6A). Mutant *cce1*Δ cells were not sensitive to the range of 4-NQO doses used, and its combination with *mph1*Δ did not further increase the sensitivity of the single *mph1*Δ (Figure 6B). Similarly, the presence of the *pif1-m1* allele did not result in a significant 4-NQO sensitivity and no further additivity was observed by combining *mph1*Δ in a double mutant (Figure 6C). The use of a *pif1*Δ null allele resulted in a strong nuclear synergistic effect (Figure 6C) suggesting specific nuclear roles of both proteins that are not conserved in the mitochondria. Combination of *mph1*Δ with either *din7*Δ or *ntg1*Δ displayed an

epistatic relationship with moderate sensitivity to 4-NQO (Figure 6C). Zeocin or MMS did not reveal a major differential impact in viability comparing YP-G to YP-D in our assay conditions. We only detected a specific MMS sensitivity in YP-G in the *abf2*Δ strains, and Zeocin treatment only impacted mildly the YP-G growth of *mph1*Δ cells (Figure 6D). While we cannot exclude mitochondrial contributions of Mph1 during the response to MMS and Zeocin, those are mostly parallel to functions in the nucleus that promote cell viability in YP-D growth conditions too. Nonetheless, the sensitivities and genetic interactions detected with 4-NQO confirm that the deletion of *MPH1* has an effect on the integrity of mitochondrial functions under conditions of DNA damage.

4. Discussion

In this work we describe a direct localization of a fraction of the Mph1 helicase to yeast mitochondria. Similar to the helicase Pif1, Mph1 presents a dual localization with a majority of the protein localizing to the nucleus and a minor fraction residing in the mitochondria. While Mph1 can be detected by western blot in mitochondrial fractions regardless of the presence of induced mtDNA, we can only detect Mph1 in the mitochondria by microscopy in the presence of mtDSB when it clusters in foci above the background level.

The role of Mph1 in the mitochondria is not essential for mtDNA maintenance in unchallenged conditions, and does not induce a significant increase in the frequency of spontaneous petite formation. The use of a mitochondrial-targeted *Xho*I allowed us to generate a highly specific mitochondrial damage without significant nuclear impact or detectable effects in cell viability under growth with fermentable carbon sources. Nonetheless, at prolonged *Xho*I expression most of the mitochondrial nucleoids enter a futile cleavage cycle after repair, and roughly 75% of the colonies from induced cells lose mtDNA integrity and its respiration competence (Figure 4). Putative impacts of mitochondrial recombination players can be better browsed at intermediate induction times, mimicking what would be a mitochondrial limited exposure to sub-lethal doses of a

radiomimetic agent. By looking at the dose-response survival curves we confirmed the role of both Mph1 and Cce1 in limiting the severity of the respiration deficiency induction after generation of mtDSBs. This role can be explained by its involvement in a mitochondrial homologous recombination pathway [12-14], but also alternatively, by its contribution to replication mechanisms used to amplify mtDNA after damage induction [5]. Impairment in such a replication mechanism will reduce the number of available copies of mtDNA and accelerate the occurrence of complete mtDNA loss during the induction of targeted mtDSBs. The persistence of a significant population of respiration competent cells after a prolonged induction of mtDSB suggests that once all molecules of the mtDNA are likely cut in the mitochondria of a given cell, there exist the possibility of repair with the existing partially processed intermediates (blunt ended broken molecules, resected molecules, partially extended molecules displaced and having ssDNA overhangs, gapped intermediates, etc.) by mechanisms of annealing and amplification still to characterize in detail. The presence of such reservoir of intermediates would be a direct consequence of the multi-copy nature of mtDNA and represent a diferent situation to that experienced in the nucleus.

While *mph1*Δ seems mostly epistatic to Ntg1 or Din7 functions, we detected a slight synergism in the deletion of both *cce1*Δ and *mph1*Δ under induced mtDSBs (Figures 4 and 5). This synergistic relationship may suggest alternative roles for Mph1 and Cce1 in dealing with either replication or recombination DNA intermediates, similarly to what occurs in the nucleus between Mus81-Mms4 and Mph1 [3].

Cells growing in the presence of limited amounts of 4-NQO showed sensitivity in conditions selecting for their respiration competence, thus allowing the study of the impact of some genetic backgrounds for mtDNA integrity and mitochondrial function. In these conditions we were able to detect a synergistic effect of the combination of *abf2*Δ and *mph1*Δ. Mph1 deletion also aggravates the spontaneous mitochondrial DNA integrity issues and the induction of respiration deficiency in *abf2*Δ strains, that have a reported increased spontaneous petite frequency [7, 60]. Absence of Abf2 has an important

structural impact in the mitochondrial nucleoids [59], and induces increased spontaneous defects in mtDNA maintenance in which Mph1 can play an attenuating role. Interestingly, such a genetic interaction is reminisicent of the functional interplay of nuclear Mph1 with the Smc5-Smc6 complex [2]. The combination of *pif1*-m1 and *mph1*Δ had a negligible impact for 4-NQO sensitivity in both YP-D or YP-G media while the double null mutant (*pif1*Δ *mph1*Δ) showed a strong synergism in both media (Figure 6C). In the nucleus, Pif1 and Mph1 have some nuclear-specific roles in the telomere maintenance [32, 63-65] thus explaining this sensitivity when both nuclear proteins are absent.

The differences between the phenotypes observed after induction of DSBs in the mtDNA and the exposure to 4-NQO, that introduces DNA adducts and impairs mtDNA replication, suggests that Mph1 can play in the mitochondria similar roles to those described in the nucleus in the template switching of replication forks in the presence of stalling-lesions [66] and in the dissociation of D-loop and strand-invasion intermediates during recombination [3].

Overall, the involvement of the Mph1 helicase in the maintenance of mtDNA stability after DNA damage aimed specifically to the mitochondria suggests a larger role of the Fanconi Anemia associated genes in the homeostasis of mitochondria and the putative impact of its mutations in the balance of endogenous oxidative stress related damages.

Author contributions

GM obtained funding and designed the experimental plan, contributed to strain generation by crossing and figures 4, 5, 6 and S2. MB generated new alleles, contributed to strain generation by crossing and contributed to Figures 1, 2, 3, 4, 5 and 6 and supplementary figures and tables. ML and XY contributed with Table 1. GM wrote the paper with contributions from ML.

Acknowledgments

Dr. Lynn Harrison (LSUHSC, USA) is gratefully acknowledged for sharing the plasmids

expressing mtRFP and mtXhoI (originated from material provided by New England Biolabs). We thank Dr. Helle Ulrich for kindly sharing the strains carrying the *pif1*-m1::TRP1 and *pif1*Δ::HphMX alleles. We thank members of the UMR 8200 of the CNRS for useful discussions. The laboratory of GM was supported by the ATIP-Avenir joint program of the CNRS and INSERM. GM laboratory was also funded with a grant from the Gustave Roussy Foundation with donations from Natixis and a grant from "Fondation ARC pour la Recherche sur le Cancer". GM is a full-time INSERM researcher at the CNRS. MB has benefited from a post-doctoral funding from LNCC (La Ligue contre le Cancer). XY was supported by a fellowship from the Chinese Scholarship Council. ML was supported by the Danish Council for Independent Research (FNU) and the Villum Foundation.

Data Availability

All data and materials of this article are available upon reasonable request. Requests for mtXhoI and mtRFP expressing plasmids should be directed to Dr. Lynn Harrison (LSUHSC, USA).

Conflict of interest

Authors declare no competing interests.

References

1. Prakash, R., et al., *Yeast Mph1 helicase dissociates Rad51-made D-loops: implications for crossover control in mitotic recombination.* Genes Dev, 2009. **23**(1): p. 67-79.
2. Chen, Y.H., et al., *Interplay between the Smc5/6 complex and the Mph1 helicase in recombinational repair.* Proc Natl Acad Sci U S A, 2009. **106**(50): p. 21252-7.
3. Mazon, G. and L.S. Symington, *Mph1 and Mus81-Mms4 prevent aberrant processing of mitotic recombination intermediates.* Mol Cell, 2013. **52**(1): p. 63-74.
4. Kang, Y.H., et al., *The MPH1 gene of Saccharomyces cerevisiae functions in Okazaki fragment processing.* J Biol Chem, 2009. **284**(16): p. 10376-86.
5. Shokolenko, I., et al., *Oxidative stress induces degradation of mitochondrial DNA.* Nucleic Acids Res, 2009. **37**(8): p. 2539-48.
6. Kucej, M., et al., *Mitochondrial nucleoids undergo remodeling in response to metabolic cues.* J Cell Sci, 2008. **121**(11): p. 1861-8.
7. O'Rourke, T.W., et al., *Mitochondrial dysfunction due to oxidative mitochondrial DNA damage is reduced through cooperative actions of diverse proteins.* Mol Cell Biol, 2002. **22**(12): p. 4086-93.
8. Doudican, N.A., et al., *Oxidative DNA damage causes mitochondrial genomic instability in Saccharomyces cerevisiae.* Mol Cell Biol, 2005. **25**(12): p. 5196-204.
9. Kazak, L., A. Reyes, and I.J. Holt, *Minimizing the damage: repair pathways keep mitochondrial DNA intact.* Nat Rev Mol Cell Biol, 2012. **13**(10): p. 659-71.
10. Wisnovsky, S., S.R. Jean, and S.O. Kelley, *Mitochondrial DNA repair and replication proteins revealed by targeted chemical probes.* Nat Chem Biol, 2016. **12**(7): p. 567-73.
11. Yogev, O. and O. Pines, *Dual targeting of mitochondrial proteins: mechanism, regulation and function.* Biochim Biophys Acta, 2011. **1808**(3): p. 1012-20.
12. Swartzlander, D.B., et al., *Regulation of base excision repair: Ntg1 nuclear and mitochondrial dynamic localization in response to genotoxic stress.* Nucleic Acids Res, 2010. **38**(12): p. 3963-74.
13. Lahaye, A., et al., *PIF1: a DNA helicase in yeast mitochondria.* EMBO J, 1991. **10**(4): p. 997-1007.
14. Stein, A., L. Kalifa, and E.A. Sia, *Members of the RAD52 Epistasis Group Contribute to Mitochondrial Homologous Recombination and Double-Strand Break Repair in Saccharomyces cerevisiae.* PLoS Genet, 2015. **11**(11): p. e1005664.
15. White, M.F. and D.M. Lilley, *The resolving enzyme CCE1 of yeast opens the structure of the four-way DNA junction.* J Mol Biol, 1997. **266**(1): p. 122-34.
16. Ling, F. and T. Shibata, *Recombination-dependent mtDNA partitioning: in vivo role of Mhr1p to promote pairing of homologous DNA.* EMBO J, 2002. **21**(17): p. 4730-40.
17. Fikus, M.U., et al., *The product of the DNA damage-inducible gene of Saccharomyces cerevisiae, DIN7, specifically functions in mitochondria.* Genetics, 2000. **154**(1): p. 73-81.
18. Williamson, D., *The curious history of yeast mitochondrial DNA.* Nat Rev Genet, 2002. **3**(6): p. 475-81.
19. Bogenhagen, D.F., *Mitochondrial DNA nucleoid structure.* Biochim Biophys Acta, 2012. **1819**(9-10): p. 914-20.
20. Lecrenier, N. and F. Foury, *New features of mitochondrial DNA replication system in yeast and man.* Gene, 2000. **246**(1-2): p. 37-48.
21. Diffley, J.F. and B. Stillman, *DNA binding properties of an HMG1-related protein from yeast mitochondria.* J Biol Chem, 1992. **267**(5): p. 3368-74.

22. Taylor, R.W. and D.M. Turnbull, *Mitochondrial DNA transcription: regulating the power supply.* Cell, 2007. **130**(2): p. 211-3.
23. Baldacci, G., B. Cherif-Zahar, and G. Bernardi, *The initiation of DNA replication in the mitochondrial genome of yeast.* EMBO J, 1984. **3**(9): p. 2115-20.
24. Xu, B. and D.A. Clayton, *A persistent RNA-DNA hybrid is formed during transcription at a phylogenetically conserved mitochondrial DNA sequence.* Mol Cell Biol, 1995. **15**(1): p. 580-9.
25. Shibata, T. and F. Ling, *DNA recombination protein-dependent mechanism of homoplasmy and its proposed functions.* Mitochondrion, 2007. **7**(1-2): p. 17-23.
26. Prasai, K., et al., *Evidence for double-strand break mediated mitochondrial DNA replication in Saccharomyces cerevisiae.* Nucleic Acids Res, 2017. **45**(13): p. 7760-7773.
27. Ling, F. and T. Shibata, *Mhr1p-dependent concatemeric mitochondrial DNA formation for generating yeast mitochondrial homoplasmic cells.* Mol Biol Cell, 2004. **15**(1): p. 310-22.
28. Ling, F., et al., *Din7 and Mhr1 expression levels regulate double-strand-break-induced replication and recombination of mtDNA at ori5 in yeast.* Nucleic Acids Res, 2013. **41**(11): p. 5799-816.
29. Hattori, N., et al., *Changes of ROS during a two-day ultra-marathon race.* Int J Sports Med, 2009. **30**(6): p. 426-9.
30. Prakash, R., et al., *Saccharomyces cerevisiae MPH1 gene, required for homologous recombination-mediated mutation avoidance, encodes a 3' to 5' DNA helicase.* J Biol Chem, 2005. **280**(9): p. 7854-60.
31. Ward, T.A., et al., *Components of a Fanconi-like pathway control Pso2-independent DNA interstrand crosslink repair in yeast.* PLoS Genet, 2012. **8**(8): p. e1002884.
32. Silva, S., et al., *Mte1 interacts with Mph1 and promotes crossover recombination and telomere maintenance.* Genes Dev, 2016. **30**(6): p. 700-17.
33. Meeusen, S., et al., *Mgm101p is a novel component of the mitochondrial nucleoid that binds DNA and is required for the repair of oxidatively damaged mitochondrial DNA.* J Cell Biol, 1999. **145**(2): p. 291-304.
34. Rendekova, J., et al., *Mgm101: A double-duty Rad52-like protein.* Cell Cycle, 2016. **15**(23): p. 3169-3176.
35. Kucejova, B. and F. Foury, *Search for protein partners of mitochondrial single-stranded DNA-binding protein Rim1p using a yeast two-hybrid system.* Folia Microbiol (Praha), 2003. **48**(2): p. 183-8.
36. Van Dyck, E., et al., *A single-stranded DNA binding protein required for mitochondrial DNA replication in S. cerevisiae is homologous to E. coli SSB.* EMBO J, 1992. **11**(9): p. 3421-30.
37. Mbantenkhu, M., et al., *Mgm101 is a Rad52-related protein required for mitochondrial DNA recombination.* J Biol Chem, 2011. **286**(49): p. 42360-70.
38. Prasai, K., et al., *Saccharomyces cerevisiae Mhr1 can bind Xho I-induced mitochondrial DNA double-strand breaks in vivo.* Mitochondrion, 2018. **42**: p. 23-32.
39. Gregg, C., P. Kyryakov, and V.I. Titorenko, *Purification of mitochondria from yeast cells.* J Vis Exp, 2009(30).
40. Nagai, T., et al., *A variant of yellow fluorescent protein with fast and efficient maturation for cell-biological applications.* Nat Biotechnol, 2002. **20**(1): p. 87-90.
41. Sung, M.K. and W.K. Huh, *Bimolecular fluorescence complementation analysis system for in vivo detection of protein-protein interaction in Saccharomyces cerevisiae.* Yeast, 2007. **24**(9): p. 767-75.
42. Sung, M.K. and W.K. Huh, *In vivo quantification of protein-protein interactions in Saccharomyces cerevisiae using bimolecular fluorescence complementation assay.* J Microbiol Methods, 2010. **83**(2): p. 194-201.

43. Tong, A.H. and C. Boone, *Synthetic genetic array analysis in Saccharomyces cerevisiae.* Methods Mol. Biol., 2006. **313**: p. 171-92.
44. Tran, P.T., A. Paoletti, and F. Chang, *Imaging green fluorescent protein fusions in living fission yeast cells.* Methods, 2004. **33**(3): p. 220-5.
45. Schindelin, J., et al., *Fiji: an open-source platform for biological-image analysis.* Nat Methods, 2012. **9**(7): p. 676-82.
46. Mayer, A., W. Neupert, and R. Lill, *Mitochondrial protein import: reversible binding of the presequence at the trans side of the outer membrane drives partial translocation and unfolding.* Cell, 1995. **80**(1): p. 127-37.
47. Brix, J., K. Dietmeier, and N. Pfanner, *Differential recognition of preproteins by the purified cytosolic domains of the mitochondrial import receptors Tom20, Tom22, and Tom70.* J Biol Chem, 1997. **272**(33): p. 20730-5.
48. Saitoh, T., et al., *Tom20 recognizes mitochondrial presequences through dynamic equilibrium among multiple bound states.* EMBO J, 2007. **26**(22): p. 4777-87.
49. Harbauer, A.B., et al., *The protein import machinery of mitochondria-a regulatory hub in metabolism, stress, and disease.* Cell Metab, 2014. **19**(3): p. 357-72.
50. Dolezal, P., et al., *Evolution of the molecular machines for protein import into mitochondria.* Science, 2006. **313**(5785): p. 314-8.
51. Neupert, W. and J.M. Herrmann, *Translocation of proteins into mitochondria.* Annu Rev Biochem, 2007. **76**: p. 723-49.
52. Schmidt, O., N. Pfanner, and C. Meisinger, *Mitochondrial protein import: from proteomics to functional mechanisms.* Nat Rev Mol Cell Biol, 2010. **11**(9): p. 655-67.
53. Mitchel, K., K. Lehner, and S. Jinks-Robertson, *Heteroduplex DNA position defines the roles of the Sgs1, Srs2, and Mph1 helicases in promoting distinct recombination outcomes.* PLoS Genet, 2013. **9**(3): p. e1003340.
54. Chen, X.J. and R.A. Butow, *The organization and inheritance of the mitochondrial genome.* Nat Rev Genet, 2005. **6**(11): p. 815-25.
55. Garcia-Rodriguez, N., R.P. Wong, and H.D. Ulrich, *The helicase Pif1 functions in the template switching pathway of DNA damage bypass.* Nucleic Acids Res, 2018. **46**(16): p. 8347-8356.
56. Symington, L.S. and R. Kolodner, *Partial purification of an enzyme from Saccharomyces cerevisiae that cleaves Holliday junctions.* Proc Natl Acad Sci U S A, 1985. **82**(21): p. 7247-51.
57. White, M.F. and D.M. Lilley, *The structure-selectivity and sequence-preference of the junction-resolving enzyme CCE1 of Saccharomyces cerevisiae.* J Mol Biol, 1996. **257**(2): p. 330-41.
58. Koprowski, P., et al., *Enhanced expression of the DNA damage-inducible gene DIN7 results in increased mutagenesis of mitochondrial DNA in Saccharomyces cerevisiae.* Mol Genet Genomics, 2003. **269**(5): p. 632-9.
59. Zelenaya-Troitskaya, O., et al., *Functions of the high mobility group protein, Abf2p, in mitochondrial DNA segregation, recombination and copy number in Saccharomyces cerevisiae.* Genetics, 1998. **148**(4): p. 1763-76.
60. Sia, R.A., et al., *Loss of the mitochondrial nucleoid protein, Abf2p, destabilizes repetitive DNA in the yeast mitochondrial genome.* Genetics, 2009. **181**(1): p. 331-4.
61. Cheng, X., S. Dunaway, and A.S. Ivessa, *The role of Pif1p, a DNA helicase in Saccharomyces cerevisiae, in maintaining mitochondrial DNA.* Mitochondrion, 2007. **7**(3): p. 211-22.
62. Foury, F. and E.V. Dyck, *A PIF-dependent recombinogenic signal in the mitochondrial DNA of yeast.* EMBO J, 1985. **4**(13A): p. 3525-30.

63. Li, J.R., et al., *Pif1 regulates telomere length by preferentially removing telomerase from long telomere ends.* Nucleic Acids Res, 2014. **42**(13): p. 8527-36.
64. Phillips, J.A., et al., *The pif1 helicase, a negative regulator of telomerase, acts preferentially at long telomeres.* PLoS Genet, 2015. **11**(4): p. e1005186.
65. Luke-Glaser, S. and B. Luke, *The Mph1 helicase can promote telomere uncapping and premature senescence in budding yeast.* PLoS One, 2012. **7**(7): p. e42028.
66. Panico, E.R., et al., *Genetic evidence for a role of Saccharomyces cerevisiae Mph1 in recombinational DNA repair under replicative stress.* Yeast, 2010. **27**(1): p. 11-27.

Figure Legends

Figure 1. Mph1 co-localizes with mitochondrial proteins after mtDNA damage (A) Images of representative diploid cells harboring a tagged copy of Mph1 with the –VC epitope and the indicated queries (Mgm101 or Rim1) tagged with the –VN epitope, with or without induction of a plasmid-encoded mt*Xho*I generating cuts at the mtDNA. Controls with no tags are also shown. Bimolecular Fluorescence Complementation (BiFC) signal was observed at 488nm. MitoTracker staining was used to highlight the mitochondrial network. The diagram shows the positions of the XhoI sites present at the mtDNA that are cleaved after mt*Xho*I induction, generating mtDSBs. (B) Average percent of cells (±s.e.m., n=3, ≥150 cells per trial) with mitochondrial BiFC signal after 2.5h induction of mt*Xho*I with 2% galactose (red column) compared to equivalent induction with 2% glucose (green column). A shaded area indicates the background level obtained using empty-tagged diploid cells. (C) Representative images of cells harboring and endogenous copy of *MPH1*-YFP after 2.5h induction of mt*Xho*I or a mock control. *mph1*Δ cells were used as control. Mph1-YFP foci co-localizing with MitoTracker staining are indicated with white arrows. The percent cells with mitochondrial foci were quantified and its average (±s.e.m.) was plotted in the bar graph shown at the right (n=3, ≥150 cells per trial). Asterisk indicates statistical significance after student's T-test (*P<0.05, **P<0.005).

Figure 2. A subset of Mph1 protein pool localizes to the mitochondria fraction. (A) protein extracts from the whole cell fraction (WC) and the purified mitochondrial fraction (Mt) obtained after sucrose gradient fractionation of un-tagged and *MPH1*-F-HA tagged strains were immunoblotted with anti-HA (upper panel). The lower part of the membranes were immunoblotted with anti-TIM23 (mitochondrial loading control) and histone H2B (nuclear loading control), respectively. (B) A strain with the endogenous MPH1-F-HA allele harboring the inducible mtXhoI was induced for 2.5h with 2% galactose (+mtDSB) or kept under repression with 2% glucose (-mtDSB). Protein fractions were obtained and

immunoblotted as in (A). Band intensity of three independent experiments was quantified to estimate the Mph1/Tim23 ratio and the fold change between the two conditions (average fold change indicated below the immunoblots). The membrane for the histone H2B immunoblot control was obtained from a separate duplicate gel migration to avoid cross-signal interference of anti-TIM23 after stripping.

Figure 3. The Mph1 protein shows a putative internal Mitochondrial Targeting Signal (MTS). (A) Schematic representation of Mph1 mRNA and the forward and reverse primers used for RT-PCR indicated with blue arrows. The start codon and a second putative start codon are indicated together with the putative MTS (black box). (B) Representative cells with either full-size Mph1-YFP or an endogenous truncation allele *Mph1(Met-111)-YFP* were observed for protein localization. MitoTracker staining was used to visualize the mitochondrial profile. (C) RT-PCR analysis of RNA extractions from cultures grown in either YP-D or YP-D under oxidative stress (+1mM H_2O_2). Products obtained using the indicated oligonucleotides on Mph1 and those obtained with a control pair (*BIM1* coding sequence) were migrated on agarose 2% gels and stained with ethidium bromide. The size range of bands that would be generated from amplification of spliced Mph1's mRNA is indicated with brackets. PCR with regular taq was used as control to discard the presence of DNA in the samples. (D) Immunobloting with anti-HA of protein extracts from the indicated strains. The right panel shows anti-HA immunoblotting of protein fractions (whole cell, WC and purified mitochondria, Mt) from cells harboring the endogenous *Mph1(Met-111)-F-HA* allele. The lower side of the membrane was immunoblotted with anti-Tim23 (mitochondrial loading control) and anti-H2B (nuclear loading control).

Figure 4. Respiration competent cells after mtDSB induction. (A) Cells with the indicated genetic background harboring a plasmid expressing mtXhoI or red fluorescent protein (RFP) as a mock control were induced with 2% galactose for 2.5h. The colonies formed in YP media with 2% glucose were replica-plated to YP media with 3% glycerol to

determine their respiration competence (ability to grow in glycerol). Bars show the average respiration competence (±s.e.m.) of cells after mtDSB induction (green bars) or its equivalent mock induction (red bars). Average values, standard deviations, number of trials and statistical analysis are summarized in tables S3 and S4. (B) On the left, a diagram showing the coding regions of *BIM1* (chromosome V) and *COX1* (mitochondrial DNA). *Xho*I, *Pvu*II (P2) and *Hind*III (H3) restriction sites and the expected fragments generated by digestion with these restriction endonucleases are indicated. The region used to produce a ^{32}P labelled probe in both sequences is indicated in red with a double underlined. On the right, southern blot analysis of samples from the indicated time points of an mtXhoI induction-and-recovery experiment. DNA from the different samples were digested with *Pvu*II and *Hind*III and separated in agarose 0.5% gels (TBE 0.5X). The sample in the first line was subjected to *in vitro* XhoI digestion to serve as standard of the expected sizes when cut by the inducible mtXhoI. An estimation of the total and the % of cut mtDNA at *COX1* (n=3) is indicated below the southern blot. (C) The amount of mtDNA was estimated by qPCR using oligonucleotides on *COX1* and normalized to the nuclear DNA content estimated by amplification with oligonucleotides on *ACT1*. Bars show the mtDNA amount fold change for the indicated strains under galactose induction (-mtDSB, red columns; +mtDSB, green columns) using the conditions of growth in YP (3% glycerol) as standard. Colony PCR was performed on individual colonies obtained after induction of mtDSB and plating in YP (2% glucose) with a pair of oligonucleotides flanking the *Xho*I site present in *COX1*.

Figure 5. **Respiration competent cells after different mtXhoI induction lengths**. (A) The graph displays the percentage of respiration competent cells (normalized to the respiration competence detected in mock conditions) after different mtXhoI induction times (15, 30, 60 and 150 min) for the indicated strains. Asterisk indicates statistical significance after student's T-test (* P<0.05, **P<0.005, *** P<0.0005) of the normalized frequencies. (B) Southern blot analysis of DNA samples of the indicated time-points of an induction of

mtDSBs in the strains with the genetic backgrounds indicated at the bottom of the gel. Samples were digested with *Pvu*II and *Hind*III and fragments detected with the combined use of probes against *COX1* and *BIM1*. Southern blots are representative of results obtained in different trials: *wild-type (n=4), mph1Δ cce1Δ (n=3), mph1Δ (n=2), cce1Δ (n=2).* An average of the quantifications is indicated. Time after induction (minutes) is indicated on top of each lane, two recovery times are indicated with +1/+2 (hours), the endpoint after over-night growth is indicated with o/n.

Figure 6. Genetic interactions of *mph1*Δ with the mtDNA maintenance genes under genotoxic stress. (A) Aliquots from YP-G (3% Glycerol) cultures of the indicated strains were plated simultaneously to YP-D (2% Glucose) or YP-G (3% Glycerol) plates containing either 0μg/ml, 0.035μg/ml, 0.06μg/ml or 0.085 μg/ml 4-NQO. After 3 days of growth colonies were counted and the surviving fraction was estimated as the percent colonies counted on the plates with the different doses reported to their respective untreated control. Each point is the average of the % survival (±s.e.m., n≥3). Average values, standard deviation, number of trials and statistics are indicated in tables S5 and S6. On the left, serial dilutions of the strains used for survival curves were spotted at the indicated doses of genotoxics in either YP-D or YP-G. (C) and (D) Serial dilutions of the indicated strains were spotted at the indicated doses of genotoxics and images were scanned after 2 days of growth for YP-D and 3 days for YP-G.

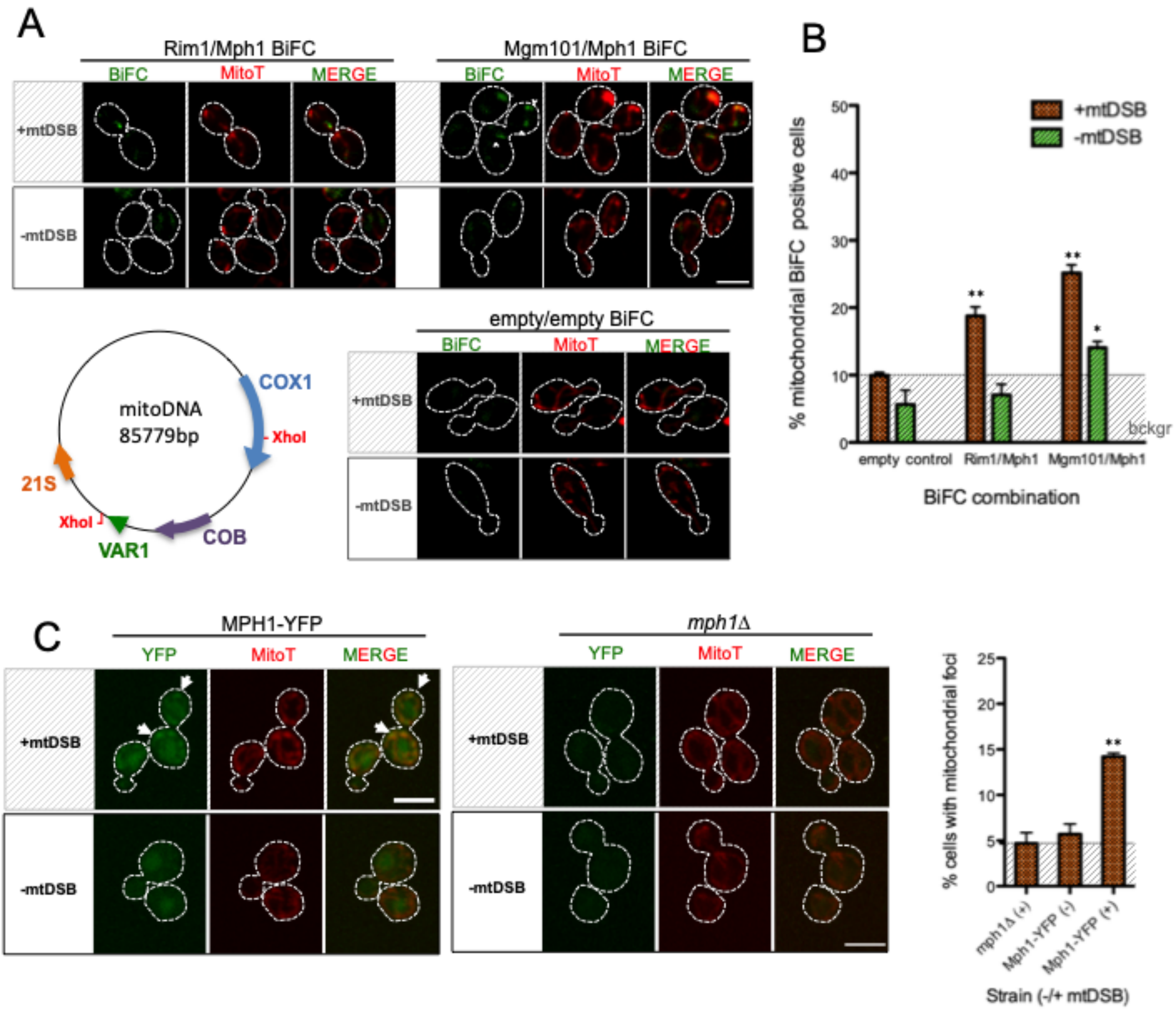
A
Rim1/Mph1 BiFC
Mgm101/Mph1 BiFC
BiFC
MitoT
MERGE
+mtDSB
-mtDSB
mitoDNA
85779bp
COX1
XhoI
21S
XhoI
COB
VAR1
empty/empty BiFC
B
% mitochondrial BiFC positive cells
+mtDSB
-mtDSB
bckgr
empty control
Rim1/Mph1
Mgm101/Mph1
BiFC combination
C
MPH1-YFP
mph1Δ
YFP
% cells with mitochondrial foci
mph1Δ (+)
Mph1-YFP (-)
Mph1-YFP (+)
Strain (-/+ mtDSB)

Figure 1

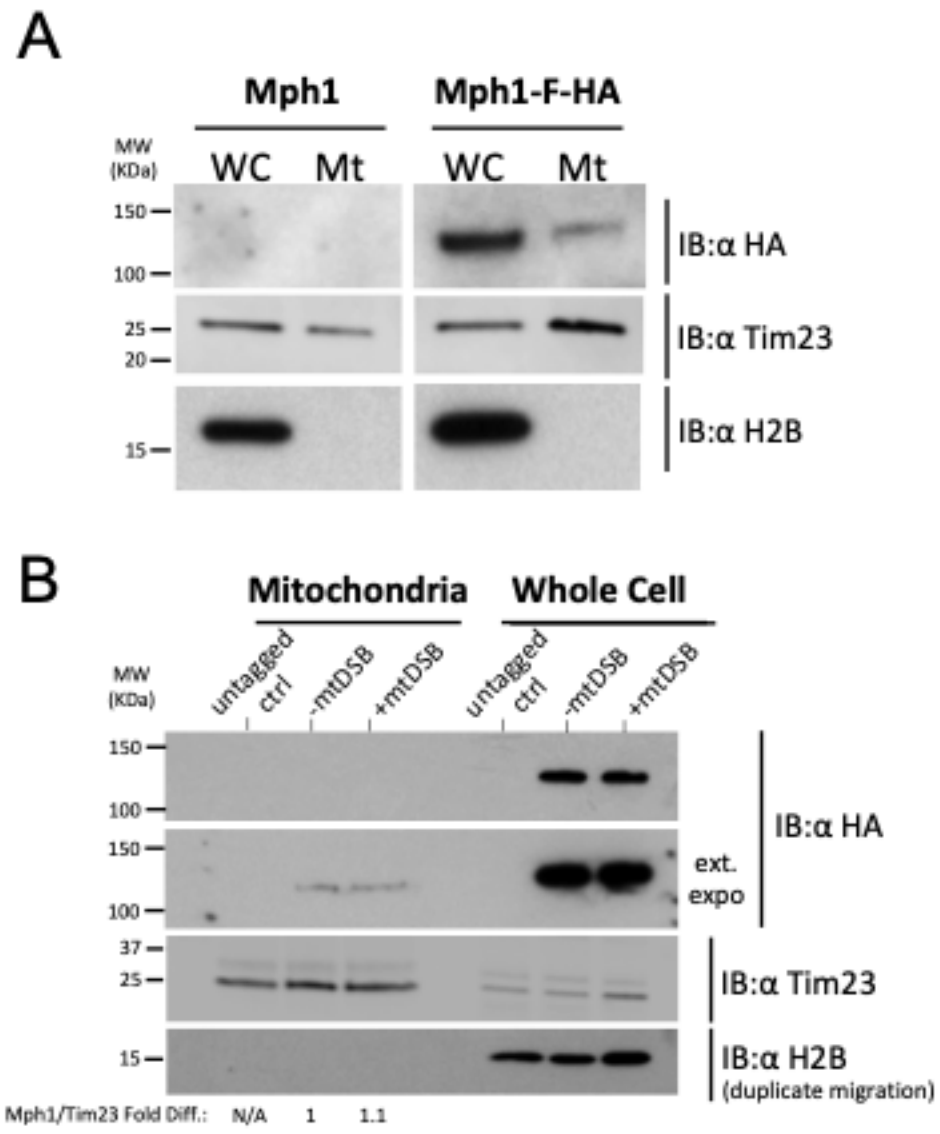
A
Mph1
Mph1-F-HA
MW (KDa)
WC
Mt
WC
Mt
150
100
25
20
15
IB:α HA
IB:α Tim23
IB:α H2B
B
Mitochondria
Whole Cell
MW (KDa)
untagged ctrl
-mtDSB
+mtDSB
untagged ctrl
-mtDSB
+mtDSB
150
100
150
100
37
25
15
ext. expo
IB:α HA
IB:α Tim23
IB:α H2B
(duplicate migration)
Mph1/Tim23 Fold Diff.: N/A 1 1.1

Figure 2

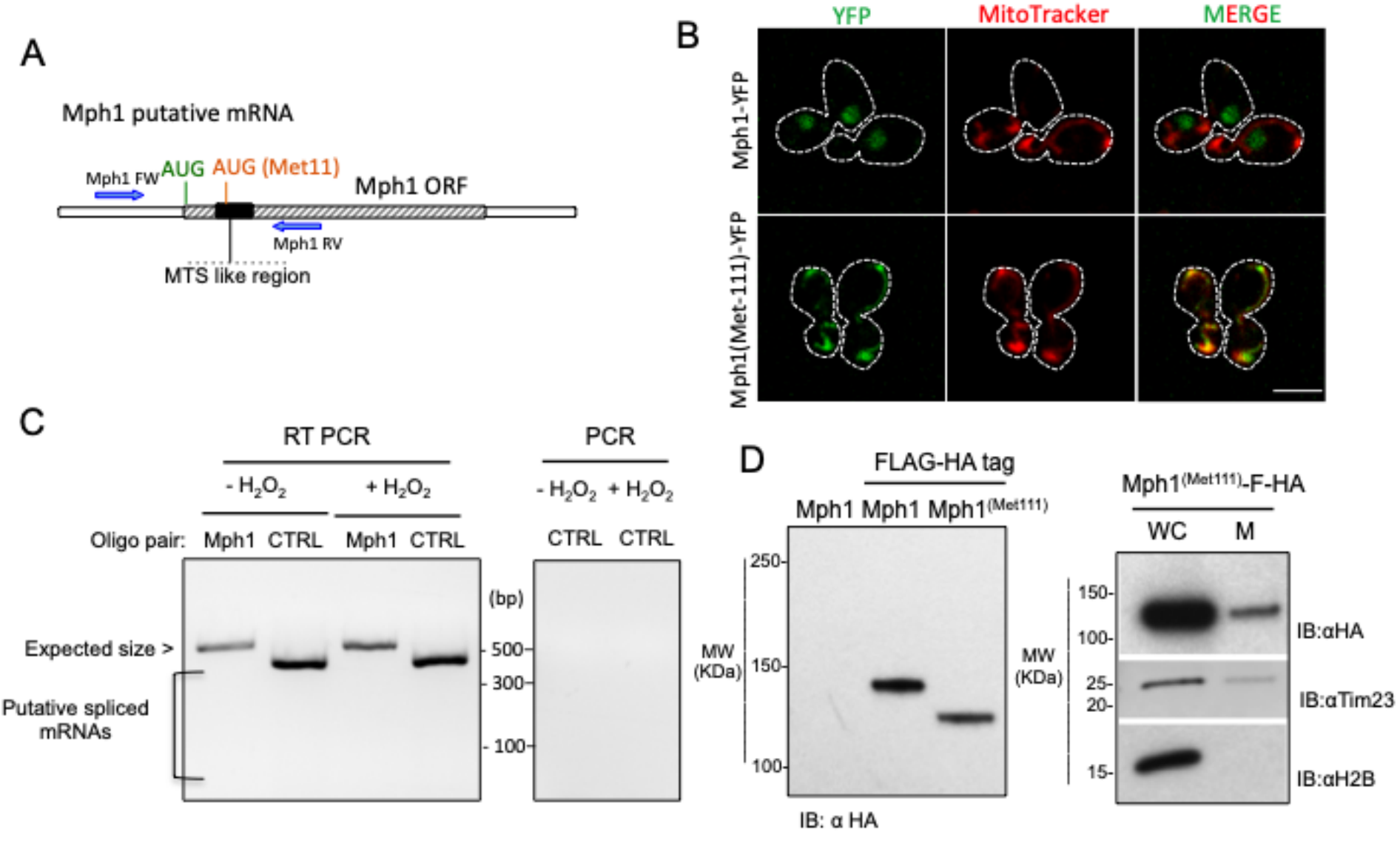
A
Mph1 putative mRNA
Mph1 FW
AUG
AUG (Met11)
Mph1 ORF
Mph1 RV
MTS like region
B
YFP
MitoTracker
MERGE
Mph1-YFP
Mph1(Met-111)-YFP
C
RT PCR
PCR
- H2O2
+ H2O2
- H2O2
+ H2O2
Oligo pair:
Mph1
CTRL
Mph1
CTRL
CTRL
CTRL
(bp)
Expected size >
Putative spliced mRNAs
500
300
100
D
FLAG-HA tag
Mph1
Mph1
Mph1(Met111)
MW (KDa)
250
150
100
IB: α HA
Mph1(Met111)-F-HA
WC
M
150
100
25
20
15
IB:αHA
IB:αTim23
IB:αH2B

Figure 3

A

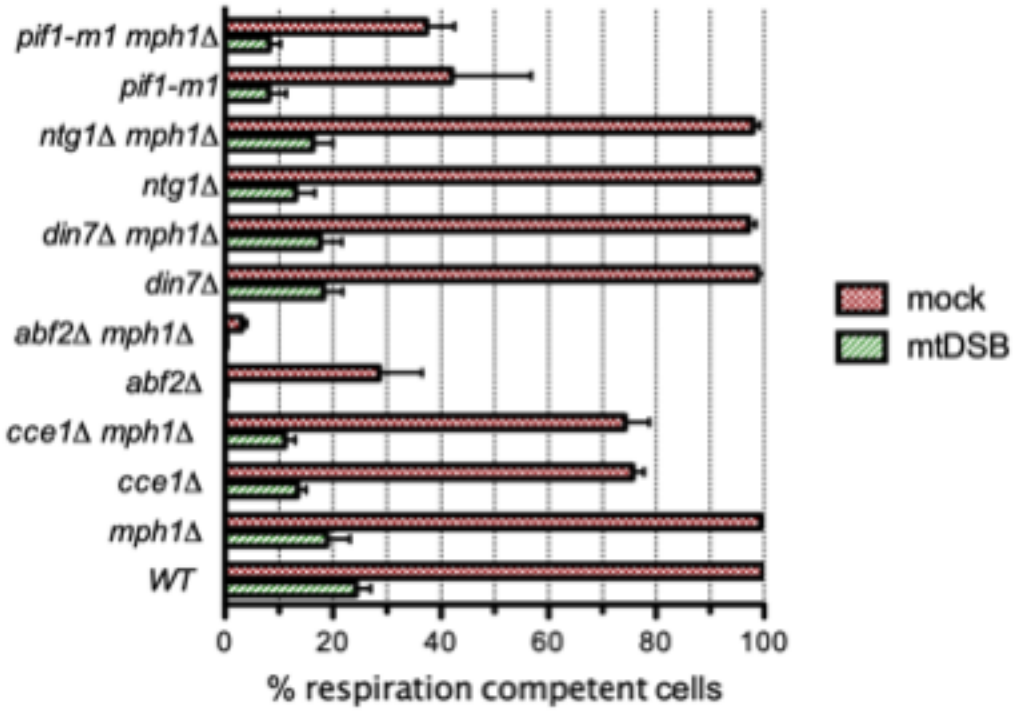
pif1-m1 mph1Δ
pif1-m1
ntg1Δ mph1Δ
ntg1Δ
din7Δ mph1Δ
din7Δ
abf2Δ mph1Δ
abf2Δ
cce1Δ mph1Δ
cce1Δ
mph1Δ
WT
0
20
40
60
80
100
% respiration competent cells
mock
mtDSB

B

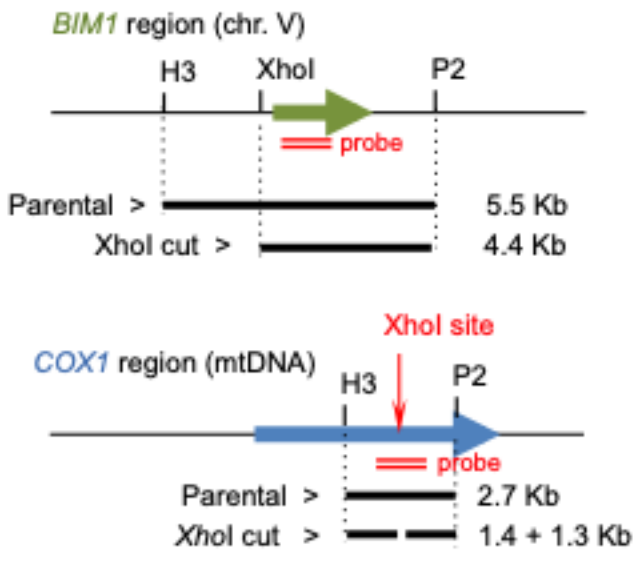
BIM1 region (chr. V)
H3
XhoI
P2
probe
Parental >
5.5 Kb
XhoI cut >
4.4 Kb
XhoI site
COX1 region (mtDNA)
H3
P2
probe
Parental >
2.7 Kb
XhoI cut >
1.4 + 1.3 Kb

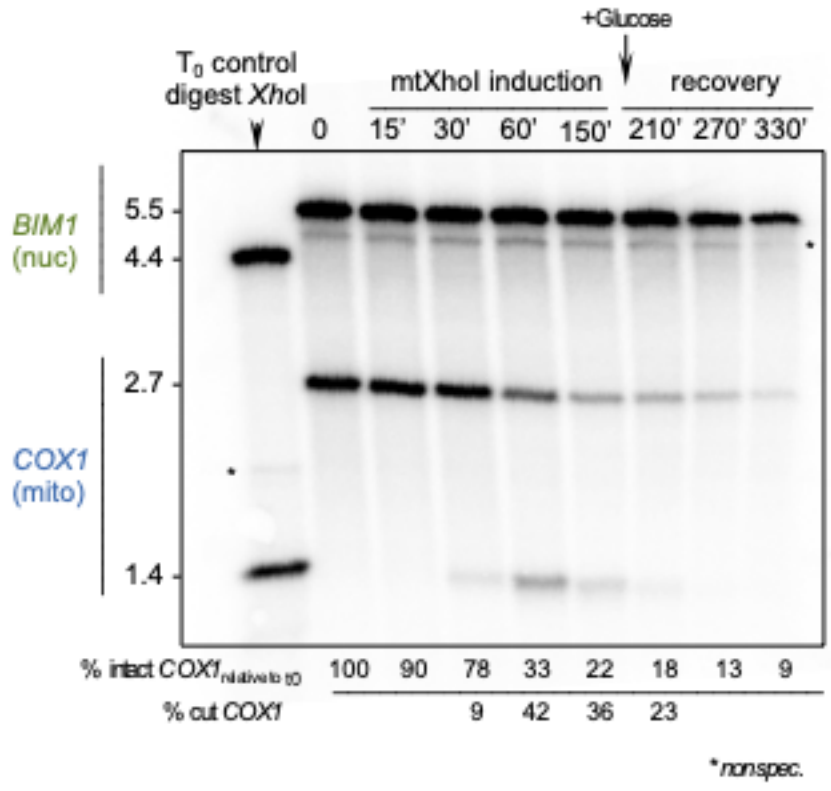
+Glucose
T0 control digest XhoI
mtXhoI induction
recovery
0
15'
30'
60'
150'
210'
270'
330'
BIM1 (nuc)
5.5
4.4
COX1 (mito)
2.7
1.4
% intact COX1 relative to t0
100
90
78
33
22
18
13
9
% cut COX1
9
42
36
23
*non spec.

C

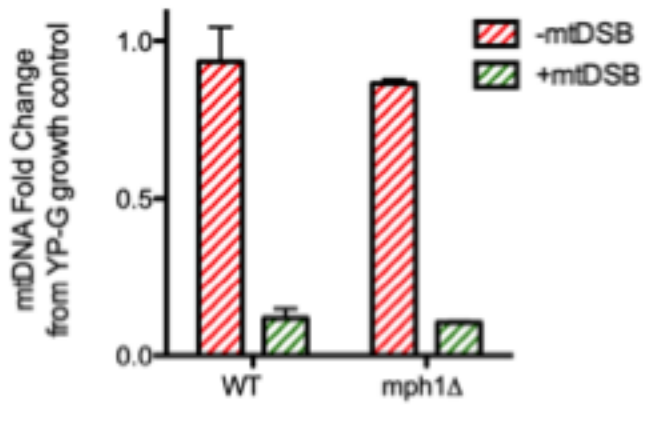
mtDNA Fold Change from YP-G growth control
1.0
0.5
0.0
-mtDSB
+mtDSB
WT
mph1Δ

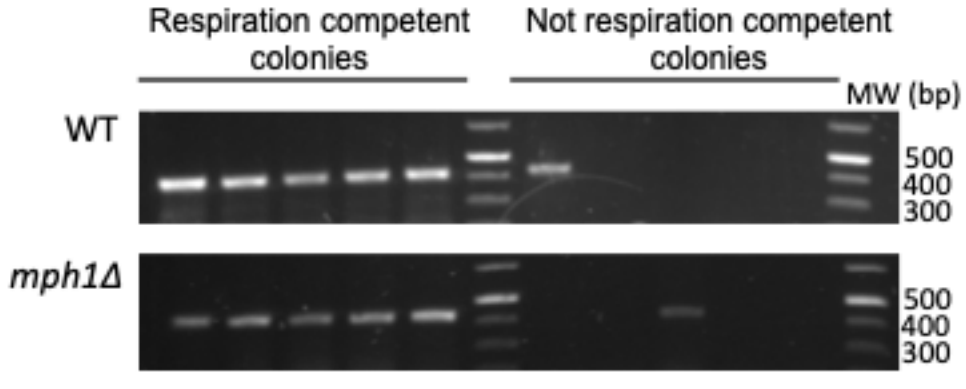
Respiration competent colonies
Not respiration competent colonies
MW (bp)
WT
mph1Δ
500
400
300
500
400
300

Figure 4

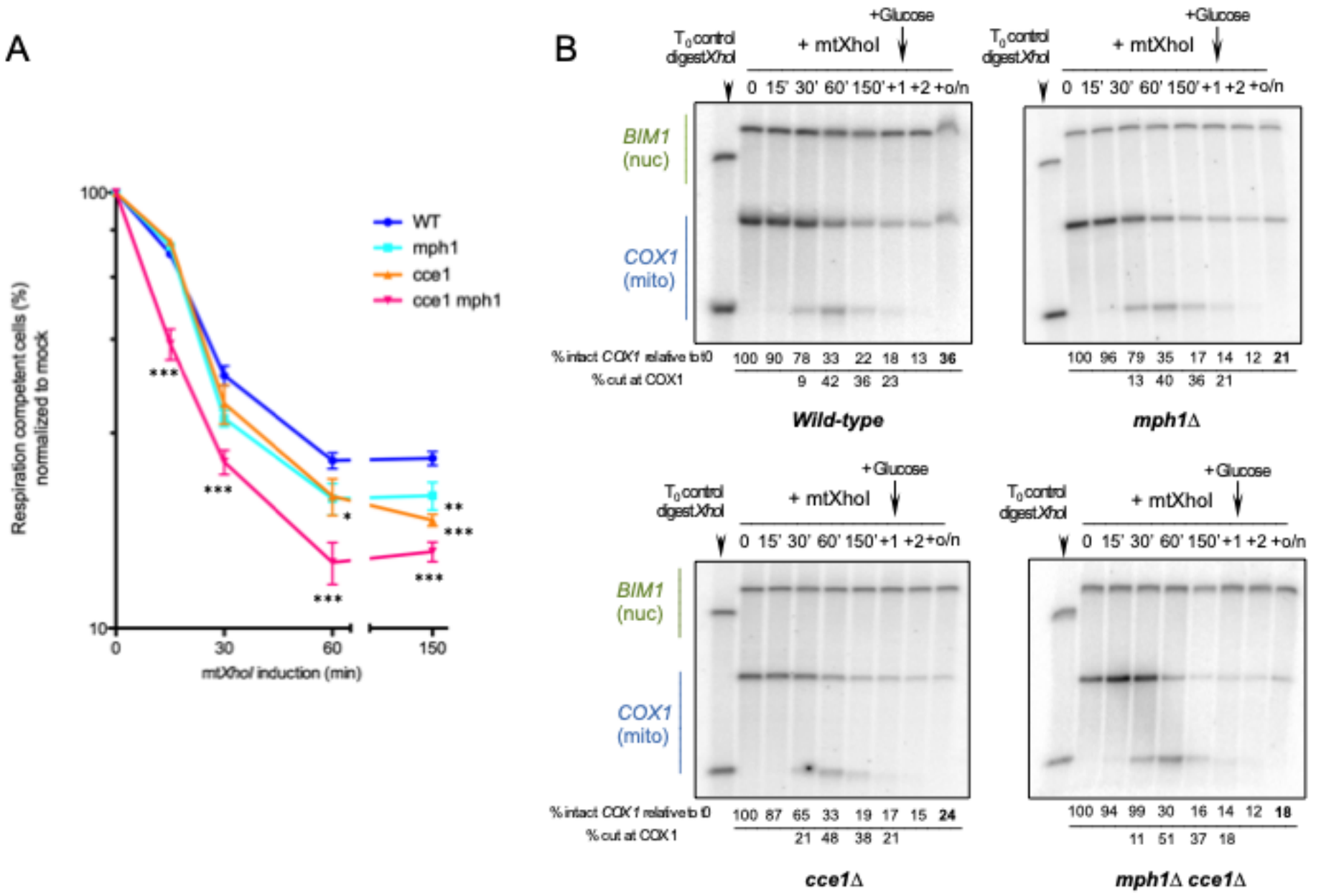
A
100
10
0
30
60
150
mtXhoI induction (min)
Respiration competent cells (%)
normalized to mock
WT
mph1
cce1
cce1 mph1
***
***
***
*
**
***
***
B
T0 control
digest Xhol
+ mtXhoI
+Glucose
0 15' 30' 60' 150' +1 +2 +o/n
BIM1
(nuc)
COX1
(mito)
% intact COX1 relative to t0
% cut at COX1
100 90 78 33 22 18 13 36
9 42 36 23
Wild-type
100 96 79 35 17 14 12 21
13 40 36 21
mph1Δ
100 87 65 33 19 17 15 24
21 48 38 21
cce1Δ
100 94 99 30 16 14 12 18
11 51 37 18
mph1Δ cce1Δ

Figure 5

A

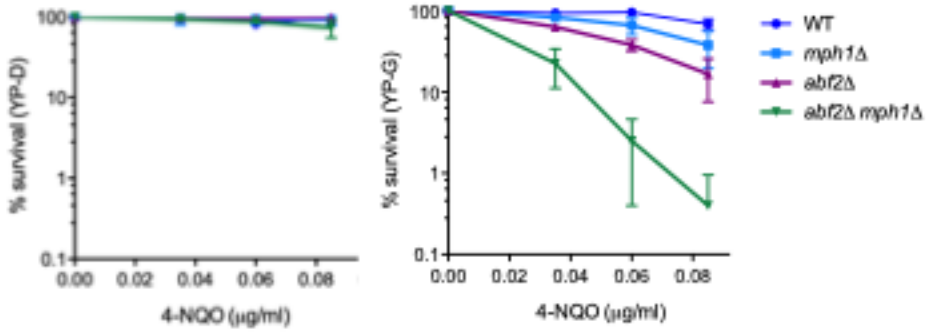

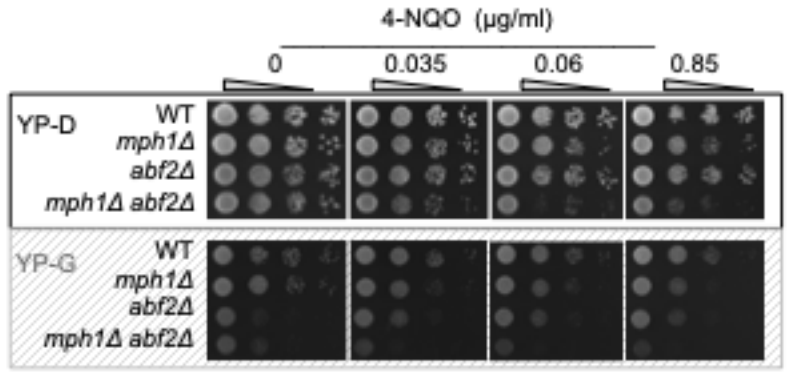

B

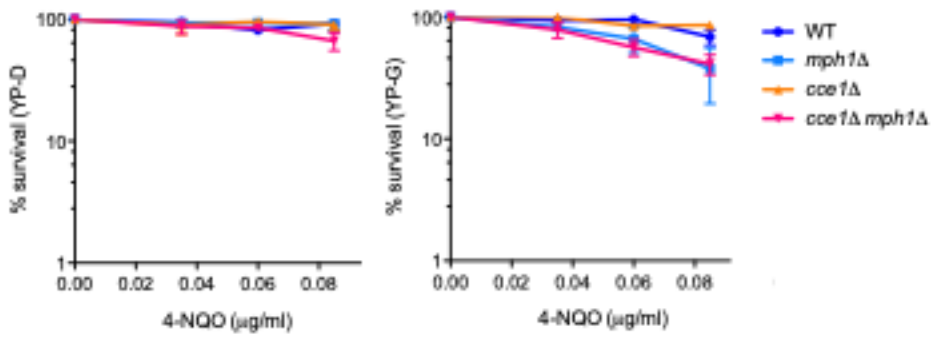

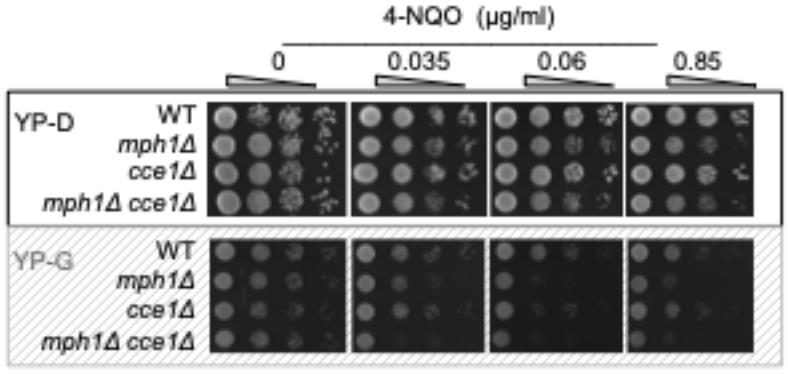

C

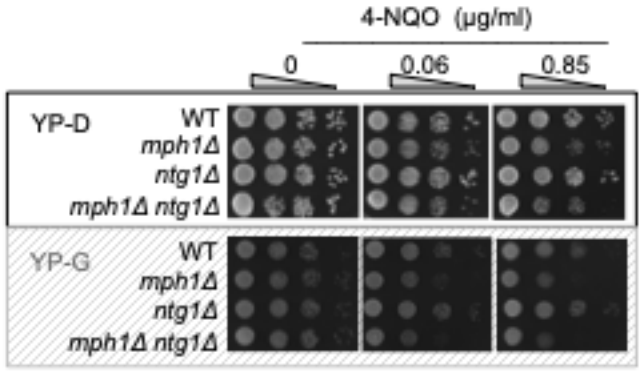

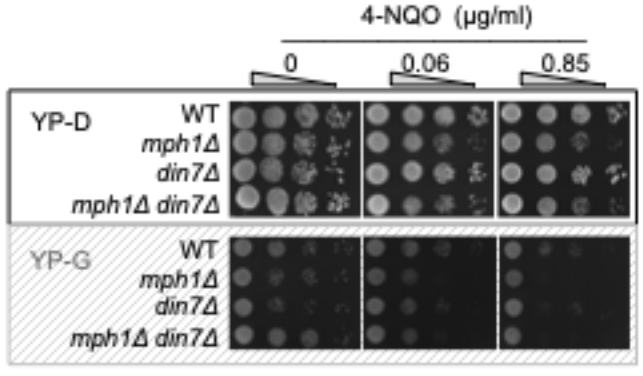

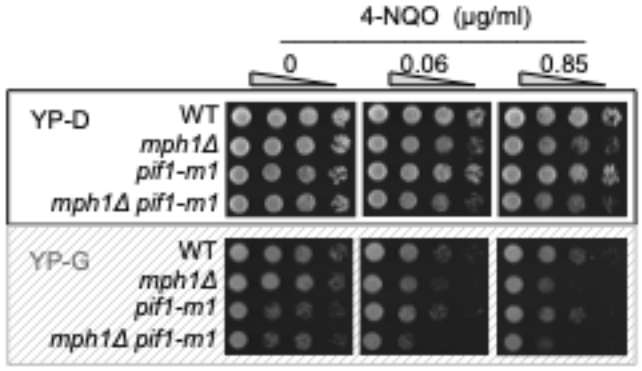

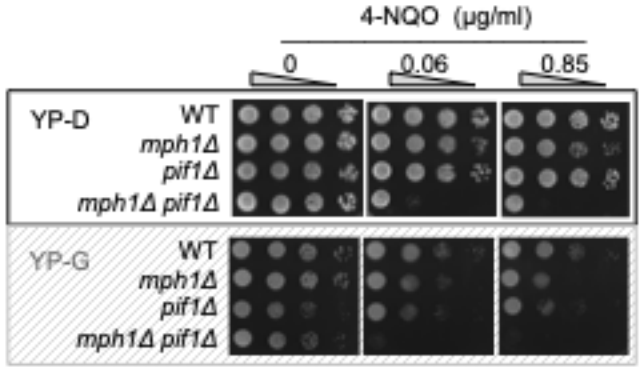

D

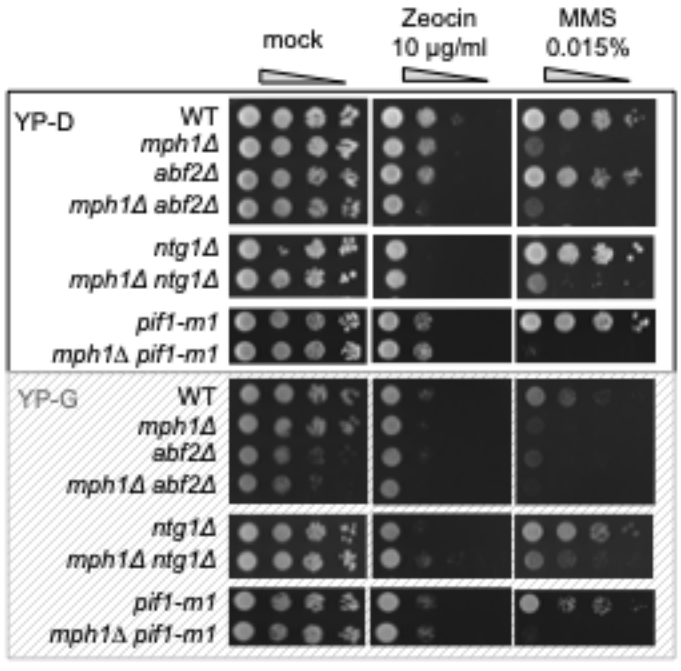

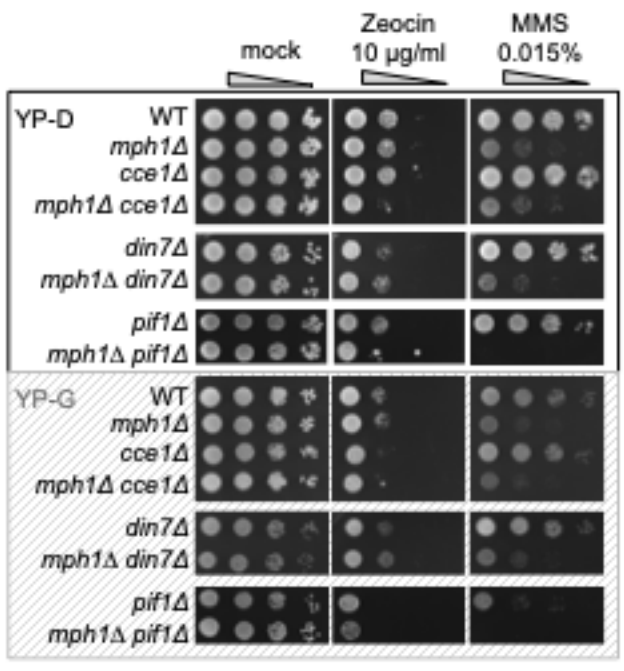

Figure 6

Table 1. Mph1 interactions from BiFC screen. Mitochondrial proteins in bold. The list shows VN-tagged proteins that produce a BiFC signal with Mph1-VC, but not with VC alone.

Bfr1	Cbc2	Cka1	Ckb1	Cof1	Cpr1
Dbp3	**Ecm18**	Hxk2	Mte1	Nhp6B	**Pda1**
Pdc5	Rpf2	Rpl29	Tif11	Tkl1	Uba1
Utp7	Ypr012W				